CORA Cork Open Research Archive
Cartlann Taighde Oscailte Chorcaí

Title	Incoherent broadband cavity-enhanced absorption spectroscopy in the near-ultraviolet: application to HONO and NO2
Authors	Gherman, Titus;Venables, Dean S.;Vaughan, Stewart;Orphal, Johannes;Ruth, Albert A.
Publication date	2008-02-01
Original Citation	Gherman, T.,Venables, D. S.,Vaughan, S.,Orphal, J., Ruth, A. A.; (2008) 'Incoherent broadband cavity-enhanced absorption spectroscopy in the near-ultraviolet: Application to HONO and NO2'. Environmental Science & Technology, 42 (3):890-895. doi: 10.1021/es0716913
Type of publication	Article (peer-reviewed)
Link to publisher's version	http://pubs.acs.org/doi/abs/10.1021/es0716913 - 10.1021/es0716913
Rights	Copyright © 2008 American Chemical Society. This document is the Accepted Manuscript version of a Published Work that appeared in final form in Environmental Science & Technology, copyright © American Chemical Society after peer review and technical editing by the publisher. To access the final edited and published work see http://pubs.acs.org/doi/abs/10.1021/es0716913
Download date	2026-11-08 11:19:36
Item downloaded from	https://hdl.handle.net/10468/796

UCC
University College Cork, Ireland
Coláiste na hOllscoile Corcaigh

Incoherent broadband cavity-enhanced absorption spectroscopy in the near-ultraviolet: Application to HONO and NO_2

Titus Gherman,[1] Dean S. Venables,[2] Stewart Vaughan,[1] Johannes Orphal[1, 3] and Albert A. Ruth[1,*]

[1]*Department of Physics and* [2]*Department of Chemistry, University College Cork, Cork, Ireland*

[3]*Permanent address: Laboratoire Interuniversitaire des Systèmes Atmosphériques, Créteil, France*

Abstract

The first application of incoherent broadband cavity-enhanced absorption spectroscopy (IBBCEAS) in the near ultraviolet for the simultaneous detection of two key atmospheric trace species, HONO and NO_2, is reported. For both compounds the absorption is measured between 360 and 380 nm with a compact cavity-enhanced spectrometer employing a high power light-emitting diode. Detection limits of ~4 ppbv for HONO and ~14 ppbv for NO_2 are reported for a static gas cell setup using a 20 s acquisition time. Based on an acquisition time of 10 min and an optical cavity length of 4.5 m detection limits of ~0.13 ppbv and ~0.38 ppbv were found for HONO and NO_2 in a 4 m^3 atmospheric simulation chamber, demonstrating the usefulness of this approach for *in situ* monitoring of these important species in laboratory studies or field campaigns.

* Corresponding author. Email: a.ruth@ucc.ie, Fax: +353-21-4276949

Introduction

Many important atmospheric trace gases possess strong absorption bands in the near-ultraviolet (near-UV) and excitation of several species in this spectral region is closely tied with important photochemical cycles in the troposphere. The near-UV photolysis of HONO, formed by *e.g.* heterogeneous chemistry involving NO_2, is a source of the primary daytime oxidant, the hydroxyl radical (OH). Hence monitoring HONO as a precursor of OH is important to furthering our understanding of tropospheric oxidation processes. The mechanisms of HONO formation in the troposphere are still not well understood (1,2). Although it is generally agreed that heterogeneous NO_2 chemistry is probably the most important source of HONO (3,4), modelled HONO concentrations are often significantly below observed values (5,6). Since the photochemistry of HONO is closely connected to that of NO_2 (7-9), whose A←X absorption band (320-660 nm) also reaches into the near-UV region, the measurement of time-dependent HONO and NO_2 mixing ratios by monitoring both species simultaneously is particularly interesting (10). Notwithstanding HONO and NO_2, there are many other atmospherically relevant species that also absorb in the near-UV, such as SO_2, H_2CO, BrO, OClO and acetone. The further development of sensitive absorption methods in the near-UV would thus benefit both field observations and laboratory studies.

Sensitive absorption spectroscopy of gases requires a long optical path. Pathlengths of up to several kilometres, as in long-path differential optical absorption spectroscopy (DOAS) and its variations (11), have been used for tropospheric sensing in the ultraviolet for several decades. A key feature of DOAS systems is their use of a relatively wide spectral window, which allows the simultaneous detection of multiple absorbing species. However, the long absorption paths utilized in DOAS systems are a disadvantage when small spatial variations in the atmosphere's composition are of interest (11-14). For atmospheric absorption measurements requiring high spatial resolution as well as high sensitivity, optically stable cavities can be used to trap light between two highly reflecting dielectric mirrors,

thereby creating a long effective absorption pathlength (15). In cavity-enhanced absorption spectroscopy, light is trapped between two highly reflecting dielectric mirrors, resulting in a long effective absorption pathlength. Among cavity-based techniques, cavity ring-down spectroscopy (CRDS) has been successfully employed for extremely sensitive field measurements of molecules with strong absorption features in the visible (16). However, using CRDS for field observations in the ultraviolet poses challenges in the design of a compact, cost-effective instrument. Monitoring multiple species with good time resolution is also difficult to realize with CRDS unless a broadband approach is taken (17).

Incoherent broadband cavity-enhanced absorption spectroscopy (IBBCEAS), an approach developed in our group (18-20), combines the flexibility of a wide spectral window with the sensitivity and compactness provided by cavity-enhanced absorption methods. Thus far, IBBCEAS has been applied solely to species absorbing in the visible region of the spectrum, for instance, to NO_2 absorbing in around 450 nm (21) and NO_3 absorbing at 662 nm (19).

The aims of the present work are (i) to extend IBBCEAS into the near-ultraviolet for the first time, (ii) to illustrate the utility of the method by focusing on the simultaneous detection of HONO and NO_2 between 360 and 380 nm in laboratory studies, and (iii) to discuss issues relating to the adoption of IBBCEAS for *in situ* field experiments in the near-UV.

Experimental

An IBBCEAS setup was used in conjunction with two different gas chambers: (1) A small 1.4 dm^3 stainless steel chamber, in the following referred to as 'chamber A'. (2) A 4 m^3 atmospheric simulation chamber described in a previous publication (19), referred to as 'chamber B'. A schematic diagram of the IBBCEAS setups is shown in Figure 1. The optical cavity in both chambers was formed by two adjustable highly reflecting mirrors (Layertec GmbH), which were attached to a vacuum chamber by flexible stainless steel bellows. The mirrors were separated by 115 cm for measurements with chamber A and by 4.5 m for chamber B. The mirrors' radius of curvature was 500 cm and their maximum reflectivity was centered at *ca.* 365 nm. Light from a 105 mW ultraviolet light-emitting diode (Omicron/Latronics) was focused into the optical cavity. The emission of the temperature stabilized light-emitting diode (LED) peaked at 365 nm and is shown in Figure 2a. Short-term variations in the total LED output intensity were about 1% for successive 10 s scans; a 1.1% decrease was observed in the output of the LED over an hour. Light exiting the cavity was focused into a spectrograph equipped with a CCD detector (Andor DV-401BV, 1024 pixels). Spectrographs with slightly different spectral dispersions were used in experiments with chamber A (Oriel MS127i) and chamber B (Newport MS125). Both spectrographs utilized a 1200-l/mm grating and a 50 μm slit width. Their different effective focal lengths resulted in resolutions of 0.35 and 0.5 nm respectively. The calibration of the wavelength scale was based on a second-order polynomial fit to eight emission lines of a low pressure Hg/Ne discharge lamp; the uncertainty of the absolute wavelength calibration was ±0.01 nm.

Although the emission of the LED at wavelengths longer than 385 nm is much weaker than that at the emission maximum, the transmission of the cavity is several orders of magnitude greater because the reflectivity of the mirrors falls off rapidly at these longer wavelengths. An ultraviolet band-pass filter (Semrock) was therefore placed between the LED and the cavity (see Figure 1) to cut the light outside

the wavelength range of interest (see Figure 2b-d). The pressure in chamber A was measured with a capacitance manometer (Leybold CTR-90) with an accuracy of *ca.* 0.05 mbar.

HONO may be formed by two different reactions under our experimental conditions (22,23):

$$NO_2 + NO + H_2O \rightleftarrows 2\ HONO \quad \text{(R1)}$$

$$2\ NO_2 + H_2O\ (+ h\nu) \rightleftarrows HONO + HNO_3 \quad \text{(R2)}$$

For reaction R2 light is not essential but it increases the reaction rate of HONO formation (24).

Chamber A was primed with water vapor and then evacuated for several hours to pressures of ~10^{-3} mbar. Subsequent introduction of *ca.* 25 mbar of a dilute NO_2/N_2 mixture (*ca.* 1:300) resulted in the immediate formation of HONO, which was readily identified by its absorption band at 368 nm (see Figure 2e (24)).[#1]

Chamber B was filled with *ca.* 6000 ppm water (measured with a Vaisala hygrometer) well in excess of NO_2 which was added at ppbv level. The gas mixture was exposed to UV and visible light. When HONO formation was observed the chamber was purged with dry air in order to lower the HONO concentration to an appropriate level for the measurement. Experiments in chamber B were performed at *ca.* 1010 mbar.

Because NO is an inherent impurity in the NO_2/N_2 mixture it is impossible to distinguish between reaction (R1) and (R2) as the primary pathway for HONO production. There was no evidence for light in the cavity lowering the mixing ratio of NO_2 during measurements with either chamber (cf. section on calibration below).

The absorption coefficient of the gas mixture inside the cavity was determined using (18):

[#1] The adjacent absorption peaks of HONO at 354 nm and 383 nm were also observed, but the signal-to-noise ratio of these absorption features was significantly worse owing to the lower LED intensity at these wavelengths.

$$\alpha(\lambda) = \frac{1}{L}\left(\frac{I_0}{I} - 1\right)(1 - R), \quad (1)$$

where $\alpha(\lambda)$ [cm^{-1}] is the absorption coefficient of the sample, R is the mirror reflectivity, L [cm] is the separation of the mirrors and I_0 and I are, respectively, the intensities of light transmitted by the cavity in the absence and presence of the absorbing species. For the measurement of I_0 chamber A was evacuated, whereas chamber B was flushed for 24 hours with dry air. I_0 was measured immediately before filling both chambers with a sample for measurements of I. All quantities in eq (1) are wavelength dependent except for L.

Calibration of the mirror reflectivity

The mirror reflectivities were calibrated (19) by relating the measured absorption of a known number density of NO_2 (n_{NO_2}) in the cavity to the absorption coefficient, $\alpha = n_{NO_2}\sigma_{NO_2}$, calculated with the literature absorption cross-section of NO_2 (σ_{NO_2}) (25), according to eq 1.

For measurements with chamber A a dilute NO_2/N_2 mixture (1:300) was made from known partial pressures of NO_2 and N_2; 5 to 20 mbar of this mixture were used for the calibration. It was found that the absorption of the mixture decreased typically by 10% over 2 min because of the adsorption of gaseous NO_2 on the walls of the chamber. The initial decrease in the absorption was not due to photolysis of NO_2 because blocking the LED light did not affect the rate of change of the absorption. Due to the decrease of NO_2 absorption, calibration measurements were taken with 20 s accumulation time immediately after introducing the mixture into the chamber. This approach gave mirror reflectivity spectra (cf. Figure 2c) of satisfactory reproducibility. Between 355 and 383 nm a fifth-order polynomial was fitted to the experimental mirror reflectivity and was used in the spectral

analysis. The effective maximum mirror reflectivity of 0.9985 was found at 365 nm. The uncertainty of the (1 – *R*) term was estimated to be about 20% based on variations between several calibrations.

For measurements with chamber B, FTIR spectra of the $\nu_1+\nu_3$ band of NO_2 were measured (19) between 2820 and 2940 cm^{-1} simultaneously with the NO_2 absorption in the near-UV under steady state conditions. The NO_2 mixing ratio was obtained from the integrated area of the FTIR absorption spectrum using the sum of the NO_2 line intensities from the HITRAN database (26) as a reference. From several calibration measurements at 4420 ppbv of NO_2 an effective maximum reflectivity of *R*=0.9994 *ca.* 367 nm was derived. For chamber A experiments the mirror reflectivity was observed to degrade at a much higher rate than for chamber B experiments, due to the significantly smaller volume of chamber A and the fact that some NO_2 was readily adsorbed on the chamber walls. This explains the different mirror performances observed in conjunction with the two different chambers.[#2]

Results and Discussion

(A) HONO and NO_2 measurements

Figure 3 shows the IBBCEAS spectrum of a HONO / NO_2 mixture in chamber A taken with an integration time of 20 s. After initial HONO formation in the cavity (see previous section) the pressure in the cell was adjusted by gradual pumping in order to obtain appropriate HONO concentrations for the absorption measurement.

Figure 4 shows the IBBCEAS spectrum of HONO and NO_2 in air at a pressure of *ca.* 1010 mbar in chamber B. It was taken with an integration time of 10 min.

The number densities of HONO and NO_2 were evaluated from fits of eq 2 to the measured absorption coefficient

$$\alpha(\lambda) = n_{\mathrm{HONO}}\sigma_{\mathrm{HONO}}(\lambda) + n_{\mathrm{NO_2}}\sigma_{\mathrm{NO_2}}(\lambda) + a\lambda + b\,, \qquad (2)$$

[#2] The manufacturer's specification of the maximum reflectivity is 0.9995.

where n_{HONO} and n_{NO_2} are the number densities [molecule cm^{-3}] and σ_{HONO} and σ_{NO_2} are the absorption cross-sections [cm^2 $molecule^{-1}$] of HONO and NO_2. The absorption cross-sections of HONO and NO_2 reported by Stutz *et al.* (24) and Burrows *et al.* (25), respectively, were convoluted with the instrument function of the spectrograph. The parameters a [cm^{-1} nm^{-1}] and b [cm^{-1}] in eq 2 account for a linearly changing unspecified background in the spectra. If the background in Figure 3 (about 2×10^{-7} cm^{-1}) arises solely from changes in the LED emission, this would correspond to a fractional decrease in the LED emission of *ca.* 2% from the measurement of I_0 to that of I. The fits of eq 2 to the overall absorption coefficient, α, for the two measurements are shown in Figure 3 and 4 (red solid lines). The fits agree well with the measured data and account for all significant absorption structures in the spectrum. The individual contributions of both species to α (dotted traces), the linear background (straight dashed trace), and the fit residuals (lower panel) are also shown in Figures 3 and 4. The number densities of HONO and NO_2 found in the fit shown in Figure 3 are $9.1 \pm 0.3\times10^{11}$ molecule cm^{-3} and $10.6 \pm 0.7\times10^{11}$ molecule cm^{-3}, respectively (in air at 1 bar and 20°C these number densities correspond to mixing ratios of 36.5 ± 1.2 ppbv and 42.4 ± 2.8 ppbv). The corresponding uncertainties from the non-linear least-square fitting are merely a measure for the quality of the fit. The true error of the number densities is dominated by systematic uncertainties discussed above. The dependence of the fit parameters on the spectral window was evaluated for several wavelength ranges between 366 nm and 380 nm (see Table 1). Depending on the width of the spectral range, the retrieved HONO number densities vary between 9.1×10^{11} and 10.0×10^{11} molecule cm^{-3}, with statistical uncertainties (one standard deviation) between 1 and 10%. The NO_2 number densities in Table 1 vary between 10.6×10^{11} and 13.4×10^{11} molecule cm^{-3}, with statistical uncertainties between 4 and 8%. This shows that the choice of the specific spectral range in the evaluation procedure is not critical and that the variations in the fit parameter values do not exceed the overall error in the HONO and NO_2 number densities (see

below). The best results (with statistical uncertainties of 1–2% for HONO and of 3–7% for NO_2) are obtained using a fitting window (366–378 nm) that includes both the HONO peak around 368 nm and the strongest NO_2 features around 376 nm (cf. Figure 3).

The error in the measured α is determined by the uncertainty contributions of each factor in eq 1. Since the uncertainty of the factor $(1 - R)$ is much larger than the uncertainties of $(\Delta I / I)$ and L, α is also accurate to within 20% (see above). In addition, the uncertainties associated with the literature absorption cross-sections are ~5% for both HONO (24) and NO_2 (25). The resulting overall uncertainties of the HONO and NO_2 number densities of *ca.* 20% are hence dominated by systematic errors of the IBBCEA method.

A signal-to-noise ratio (SNR) of 17 for the chamber A measurement was estimated by dividing the largest absorption difference in the relevant absorption range by the 1σ rms value of the residuals (2.0×10^{-8} cm^{-1}) of the fit. Assuming a 2:1 SNR to be sufficient for unambiguously identifying HONO and NO_2, the corresponding detection limits for both species are ~4 ppbv and ~14 ppbv respectively. These limits are based on a 20 s integration time according to the measurement in Figure 3. Based on these findings a detection limit of ~0.19 ppbv for HONO can be expected for chamber B experiments for integration times of 10 min and a resonator length of 4.5 m. Similarly for NO_2, a detection limit of ~0.66 ppbv is plausible under the same conditions. Finally, further improvement is possible using cavities with a higher finesse than in chamber A experiments (27).

The absorption spectrum in Figure 4 was measured with a 10 min integration time using chamber B (cavity length: 4.5 m). It exhibits a greater SNR than the spectrum in Figure 3, even though the retrieved mixing ratios for HONO (2.7 ± 0.1 ppbv) and NO_2 (2.4 ± 0.1 ppbv) are lower than in the chamber A measurement. From the SNR≈44 for HONO and the SNR≈16 for NO_2 detection limits of

≈0.13 ppbv and ≈0.30 ppbv can be estimated based on a SNR of 2:1. This result is in good agreement with our estimate based on the chamber A experiments. The fact that chamber A experiments were performed at low pressure as opposed to chamber B experiments did not affect the anticipated detection limits since additional losses due to Rayleigh scattering are negligibly small in comparison to (1-*R*) – see discussion below. In fact chamber B experiments were more straightforward to perform due to the significantly larger volume to surface ratio of chamber B in comparison to chamber A. Wall losses of NO_2 were significantly reduced in chamber B leading to an overall better mirror performance because the reflectivities were virtually not affected through filling chamber B. This is the reason why detection limits for the chamber B experiment are slightly smaller than estimated from chamber A experiments.

The detection limit of the chamber B experiment can be compared with those of numerous other approaches to monitor HONO: (i) *Optical methods*: Long-path DOAS systems have been used to monitor HONO and NO_2 in the atmosphere for several decades (28-31). A typical LP-DOAS system with an optical path of about 1000 m has detection limits of ~0.1 ppbv to HONO and ~0.6 ppbv to NO_2 for an acquisition time of *ca.* 20 min. Atmospheric HONO has also been detected using infrared diode-laser spectroscopy (32) with a detection limit of 0.3 ppbV averaged over 30 min, using a White cell with an optical path of 126 m. In the laboratory Fourier transform infrared spectroscopy (33) and cavity ring-down spectroscopy (34) have also been used for absorption measurements of HONO with detection limits of ~5 ppbv for acquisition times of *ca.* 20 min and 15 s, respectively. (ii) *Wet chemical methods*: Techniques employing wet chemical sampling followed by chromatographic approaches (35-37) or UV detection (38), and methods using diffusion denuders in combination with ion chromatography (39-45) generally possess smaller detection limits than optical methods, but may have very long sampling times (46). Short integration times in conjunction with ultra-high detection limits have been reported for a technique that uses wet chemical sampling in combination with long-path

absorption photometeric (LOPAP) detection. For a 4 min integration time detection limits of 3-6 pptv have been achieved with this method (38,47). Recently Beine *et al.* have reported a 3σ detection limit of <0.5 pptv for an acquisition time of *ca.* 5 min (37) through derivatization and subsequent HPLC separation. With a similar approach Huang *et al.* (36) reported a detection limit of ~1 pptv in a sampling time of *ca.* 2 min. (iii) *Other methods*: Measurement of chemiluminescence, as routinely used in NO_x monitors for the detection of NO_2 with typical sensitivities below 0.1 ppbv in a 1 min sampling time, can also be applied to the detection of HONO (48,49). Recently Liao *et al.* (50) achieved a detection limit for HONO of 10 pptv in 10 min by measuring the fluorescence of OH after laser-based photo-fragmentation of HONO. Finally, another new approach uses thermal dissociation of HONO coupled with chemiluminescent detection of NO for the detection of HONO (51).

The choice of detection method for HONO and NO_2 does not only depend on the ultimate detection limit of the instrumental approach, but also on the constraints concerning the experimental environment and the requirements and goals of a specific application. In this context near-UV IBBCEAS is characterized by several favourable features: (i) Both open and closed path configurations are possible with this approach. Open path measurements do not depend on the extraction of gases and are therefore immune from inlet wall losses that are difficult to quantify. Alternatively, in closed path experiments with IBBCEAS the sample input can be controlled by filtering aerosols or by including a chemical reactor in the input stream. (ii) The approach measures local mixing ratios and has a high spatial resolution. (iii) The simultaneous detection of multiple species is possible. (iv) Chemically interfering species, which mostly affect wet chemical approaches (35,38,50-52), can be accounted for in the data analysis.

The results presented above show that the IBBCEAS instrument presented here is appropriate for simultaneous measurement of HONO and NO_2 in polluted urban air masses, where early morning mixing ratios of up to 10 ppbv HONO (43) and over 100 ppbv NO_2 (31) may occur. Since the

concentrations of both species inside houses (13) and vehicles (14) can be several times higher than these levels, the IBBCEAS approach could also be used for indoor *in situ* measurements. The technique will also be useful in laboratory studies of these species and for real-time measurements across atmospheric simulation chambers, as demonstrated here.

(B) Practical aspects of IBBCEAS in the near UV

While the principle of IBBCEAS is equally applicable in the ultraviolet as in the visible region of the spectrum, both the choice of the light source, and the optimization of the mirror reflectivity in conjunction with increased UV scattering losses, need to be considered.

Light source: In the near UV high intensity broadband light sources, such as arc lamps, are on the one hand very flexible in terms of their use in different spectral regions, on the other hand they require careful spectral filtering of the excitation light in order to minimize stray light levels in the spectrograph. The background light level in the spectrograph is particularly problematic because the relative transmission of the cavity outside the high reflectivity range of the dielectric mirrors is several orders of magnitude higher than the transmission at the centre of the mirror reflectivity. In comparison, high power UV-LEDs, as in the present setup, offer the advantage of a relatively narrow spectral output and therefore require less stringent filtering. (Even though the LED used in this work has a narrow emission band, some light is transmitted through the cavity to the long-wavelength side of the main LED output (cf. Figure 2d, ~390 nm)). LEDs have other practical advantages including excellent short and long-term stability, compactness, and low power consumption (53,54). Indeed, Ball *et al.* (55) recently also reported the use of a high power LED in an IBBCEAS experiment in the visible. Furthermore, Kern *et al.* (56) have demonstrated the use of LEDs in a LP-DOAS system, which traditionally have used arc lamps as light sources.

Mirror reflectivities: The sensitivity of the instrument is determined by the reflectivity losses per pass (1-*R*) as long as other losses are small in comparison. Higher mirror reflectivities or longer cavity lengths do not necessarily improve the instrument's sensitivity, especially in the near UV, where increasing losses caused by extinction processes in the sample become significant. It is therefore important to compare the value of (1-*R*) ≈ 0.0006 of the present chamber B setup with typical losses per pass due to extinction processes occurring in the atmosphere around 360 nm. At this wavelength, Rayleigh scattering causes an extinction of roughly 8×10^{-7} cm^{-1} (57) in air, while a typical extinction value based on Mie scattering in a polluted urban atmosphere is roughly 1×10^{-6} cm^{-1} (58). These values correspond to losses per pass of about 0.0004 and 0.00045, respectively, for the present cavity and are still smaller than the value of (1-*R*) for chamber B experiments. Hence, Rayleigh scattering losses did not affect the measurements with the longer cavity.

The losses per pass of highly abundant gases with reasonably large cross-sections in the near UV (λ>350 nm) are generally small in comparison with (1-*R*) under normal atmospheric conditions without unusually large pollution levels including aerosols. For instance, in order to significantly shorten the effective pathlength by 10% and hence affect the sensitivity of a potential field device, NO_2 mixing ratios would have to be on the order of ~100 ppbv. The error in the retrieval of the HONO mixing ratio will, however, generally increase with increasing NO_2/HONO concentration ratios. Deeper in the UV the losses per pass due to absorption by ubiquitous gases, such as ozone, are also not necessarily negligible and need to be considered in the design of an IBBCEAS instrument. For instance, 72 ppbv of ozone produce a loss per pass of approximately 0.01 in a resonator of 5 m length around its absorption maximum at 255 nm. For this scenario mirror reflectivities of *R*>0.99 or resonators longer than 5 m will worsen the signal-to-noise ratio and hence the sensitivity of the setup if a molecule other than ozone is of interest.

Generally, the sensitivity enhancement of IBBCEAS in comparison with single pass absorption setups is larger at longer wavelengths, where Rayleigh scattering is reduced, and in clean atmospheres where aerosol losses are small.

Acknowledgements

We are very grateful to Dr. John Wenger for making the simulation chamber in the CRAC group (Chemistry Department, UCC) available to us for further measurements on the *in situ* detection of HONO. This work was supported through the Marie Curie Programme (TOK) under Framework 6 of the European Union (contract MTKD-CT-2004-014406 "Transfer of Expertise in Atmospheric Monitoring of Urban Pollutants"). Support through Science Foundation Ireland (06/RFP/CHP055) is also gratefully acknowledged.

References

(1) Calvert, J. G.; Yarwood, G.; Dunker, A. M. An evaluation of the mechanism of nitrous acid formation in the urban atmosphere. *Res. Chem. Intermed.* **1994**, *20*, 463–52.

(2) Finlayson-Pitts, B. J.; Wingen, L. M.; Sumner, A. L.; Syomin, D.; Ramazan, K. A. The heterogeneous hydrolysis of NO_2 in laboratory systems and in outdoor and indoor atmospheres: 20 An integrated mechanism. *Phys. Chem. Chem. Phys.* **2003**, *5*, 223–242.

(3) Harrison, R. M.; Kitto, A.-M. N. Evidence for a surface source of atmospheric nitrous acid. *Atmos. Environ.* **1994**, *28*, 1089–1094.

(4) Reisinger, A. R. Observation of HNO_2 in the polluted winter atmosphere: possible heterogeneous production on aerosols. *Atmos. Environ.* **2000**, *34*, 3865–3874.

(5) Vogel, B.; Vogel, H.; Kleffmann, J.; Kurtenbach, R. Measured and simulated vertical profiles of nitrous acid – Part II. Model simulations and indications for a photolytic source. *Atmos. Environ.* **2003**, *37*, 2957–2966.

(6) Lammel, G.; Cape, J. N. Nitrous acid and nitrite in the atmosphere. *Chem. Soc. Rev.* **1996**, 361–369.

(7) Johnston, H. S.; Graham, R. Photochemistry of NO_x and HNO_x compounds. *Can. J. Chem.* **1974**, *52*, 1415–1423.

(8) Aumont, B.; Chervier, F.; Laval, S. Contribution of HONO sources to the $NO_x/HO_x/O_3$ chemistry in the polluted boundary layer. *Atmos. Environ.* **2003**, *37*, 487–498.

(9) Bröske, R.; Kleffmann, J.; Wiesen, P. Heterogeneous conversion of NO_2 on secondary organic aerosol surfaces: A possible source of nitrous acid (HONO) in the atmosphere? *Atmos. Chem. Phys.* **2003**, *3*, 469–474.

(10) Kleffmann, J.; Kurtenbach, R.; Lörzer, J.; Wiesen, P.; Kalthoff, N.; Vogel, B.; Vogel, H. Measured and simulated vertical profiles of nitrous acid – part I: field measurements. *Atmos. Environ.* **2003**, *37*, 2949–2955.

(11) Platt, U. Modern methods of the measurement of atmospheric trace gases. *Phys. Chem. Chem. Phys.* **1999**, *1*, 5409–5415.

(12) Saiz-Lopez, A.; Plane, J. M. C.; McFiggans, G.; Williams, P. I.; Ball, S. M.; Bitter, M.; Jones, R. L.; Hongwei, C.; Hoffmann, T. Modelling molecular iodine emissions in a coastal environment: the link to new particle formation. *Atmos. Chem. Phys.* **2006**, *6*, 883–895.

(13) Brauer, M.; Ryan, P. B.; Suh, H. H.; Koutrakis, P.; Spengler, J. D.; Leslie, N. P.; Billick, I. H. Measurements of nitrous acid inside two research houses. *Environ. Sci. Technol.* **1990**, *24*, 1521–1527.

(14) Febo, A.; Perrino, C. Measurement of high concentrations of nitrous acid inside automobiles. *Atmos. Environ.* **1995**, *29*, 345–351.

(15) Paldus, B. A.; Kachanov, A. A. An historical overview of cavity enhanced methods. *Can. J. Phys.* **2005**, *83*, 975–999.

(16) Brown, S. S.; Stark, H.; Ciciora, S. J.; McLaughlin, R. J.; Ravishankara, A. R. Simultaneous in situ detection of atmospheric NO_3 and N_2O_5 via cavity ring-down spectroscopy. *Rev. Sci. Instrum.* **2002**, *73*, 3291–3301.

(17) Ball, S. M.; Jones, R. L. Broad-Band Cavity Ring-Down Spectroscopy. *Chem. Rev.* **2003**, *103,* 5239–5262.

(18) Fiedler, S. E.; Hese, A.; Ruth, A. A. Incoherent broad-band cavity-enhanced absorption spectroscopy. *Chem. Phys. Lett.* **2003**, *371*, 284–294.

(19) Venables, D. S.; Gherman, T.; Orphal, J., Wenger, J. C.; Ruth, A. A. High sensitivity *in situ* monitoring of NO_3 in an atmospheric simulation chamber using incoherent broadband cavity-enhanced absorption spectroscopy. *Environ. Sci. Technol.* **2006**, *40*, 6758–6763.

(20) Ruth, A. A.; Orphal, J.; Fiedler, S. E. Cavity Enhanced Fourier Transform Absorption Spectroscopy using an Incoherent Broadband Light Source. *Appl. Opt.* **2007**, *46*, 3611–3616.

(21) Langridge, J. M.; Ball, S. M.; Jones, R. L. A compact broadband cavity enhanced absorption spectrometer for detection of atmospheric NO_2 using light emitting diodes. *Analyst* **2006**, *131*, 916–922.

(22) Finlayson-Pitts, B. J.; Pitts Jr., J. N. Chemistry of the Upper and Lower Atmosphere. Academic Press, San Diego, **2000**, 269–272.

(23) Calvert, J. G.; Yarwood, G.; Dunker, A. M. An evaluation of the mechanism of nitrous-acid formation in the urban atmosphere. *Res. Chem. Intermed.* **1994**, *20*, 463–502.

(24) Ramazan, K. A.; Syomin, D.; Finlayson-Pitts, B. J. The photochemical production of HONO during the heterogeneous hydrolysis of NO_2. *Phys. Chem. Chem. Phys.* **2004**, *6*, 3836–3843.

(24) Stutz, J.; Kim, E. S.; Platt, U.; Bruno, P.; Perrino, C.; Febo A. UV-visible absorption cross-sections of nitrous acid. *J. Geophys. Res.* **2000**, *105*, 14585–14592.

(25) Burrows, J. P.; Dehn, A.; Deters, B.; Himmelmann, S.; Richter, A.; Voigt, S.; Orphal, J. Atmospheric remote-sensing reference data from GOME: 1. Temperature-dependent absorption cross sections of NO_2 in the 231–794 nm range. *J. Quant. Spectrosc. Rad. Transf.* **1998**, *60*, 1025–1031.

(26) Rothman, L. S.; Jacquemart, D.; Barbe, A.; Benner, D. C.; Birk, M.; Brown, L. R.; Carleer, M. R.; Chackerian Jr., C.; Chance, K. V.; Dana, V.; Devi, V. M.; Flaud, J.–M.; Gamache, R. R.; Goldman, A.; Hartmann, J.–M.; Jucks, K. W.; Maki, A. G.; Mandin, J.–Y.; Massie, S.; Orphal, J.; Perrin, A.; Rinsland, C. P.; Smith, M. A. H.; Toth, R. A.; Vander Auwera, J.; Varanasi, P.; Wagner, G. The HITRAN 2004 molecular spectroscopic database. *J. Quant. Spectrosc. Rad. Trans.* **2005**, *96*, 139–204.

(27) Fiedler, S. E.; Hese, A.; Ruth, A. A. Incoherent broad-band cavity-enhanced absorption spectroscopy of liquids. *Rev. Sci. Instrum.* **2005**, *76*, 023107 and **2005**, *76*, 089901 (Err.).

(28) Perner, D.; Platt, U. Detection of nitrous acid in the atmosphere by differential optical absorption. *Geophys. Res. Lett.* **1979**, *6*, 917–920.

(29) Platt, U.; Perner, D.; Harris, G. W.; Winer, A. M.; Pitts, J. N. Observations of nitrous acid in an urban atmosphere by differential optical absorption. *Nature* **1980**, *285*, 312–314.

(30) Harris, G. W.; Carter, W. P. L.; Winer, A. M.; Pitts, J. N.; Platt, U.; Perner, D. Observations of nitrous acid in the Los Angeles atmosphere and implications for the predictions of ozone-precursor relationships. *Environ. Sci. Technol*. **1982**, *16*, 414–419.

(31) Alicke, B.; Platt, U.; Stutz, J. Impact of nitrous acid photolysis on the total hydroxyl radical budget during the Limitation of Oxidant Production/Pianura Padana Produzione di Ozono study in Milan. *J. Geophys. Res. D* **2002**, *107*, 8196, doi:10.1029/2000JD000075.

(32) Schiller, C. L.; Locquiao, S.; Johnson, T. J.; Harris, G. W. Atmospheric measurements of HONO by tunable diode laser absorption spectroscopy. *J. Atm. Chem.* **2001**, *40*, 275–293.

(33) Hanst, P. L.; Wong, N. W.; Bragin, J. A long path infra-red study of Los Angeles smog. *Atmos. Environ.* **1982**, *5*, 969–981.

(34) Wang, L; Zhang, D. Detection of Nitrous Acid by Cavity Ring-Down Spectroscopy. *Environ. Sci. Technol.* **2000**, *34*, 4221–4227.

(35) Zhou, X. L.; Qiao, H. C.; Deng, G. H.; Civerolo, K. A method for the measurement of atmospheric HONO based on DNPH derivatization and HPLC analysis. *Environ. Sci. Tech.* **1999**, *33*, 3672–3679.

(36) Huang, G.; Zhou, X.; Deng, G.; Qiao, H.; Civerolo, K. Measurements of atmospheric nitrous acid and nitric acid. *Atmos. Environ.* **2002**, *36*, 2225–2235.

(37) Beine, H. J.; Amoroso, A.; Esposito, G.; Sparapani, R.; Ianniello, A.; Georgiadis, T.; Nardino, M.; Bonasoni, P.; Cristofanelli, P.; Dominé, F. Deposition of atmospheric nitrous acid on alkaline snow surfaces. *Geophys. Res. Lett.* **2005**, *32*, L10808.

(38) Heland, J.; Kleffmann, J.; Kurtenbach, R.; Wiesen, P. A new instrument to measure gaseous nitrous acid (HONO) in the atmosphere. *Environ. Sci. Technol.* **2001**, *35*, 3207–3212.

(39) Ferm, M.; Sjödin, A. A sodium carbonate coated denuder for determination of nitrous acid in the atmosphere. *Atmos. Environ.* **1985**, *19*, 979–983.

(40) Večeřa, Z.; Dasgupta, P. K. Measurement of ambient nitrous acid and a reliable calibration source for gaseous nitrous-acid. *Env. Sci. Techn.* **1991**, *25*, 255–260.

(41) Simon, P. K.; Dasgupta, P. K. Continuous automated measurement of gaseous nitrous and nitric-acids and particulate nitrite and nitrate. *Env. Sci. Tech.* **1995**, *29*, 1534–1541.

(42) Oms, M. T.; Jongejan, P. A. C.; Veltkamp, A. C.; Wyers, G. P.; Slanina, J. Continuous monitoring of atmospheric HCl, HNO_2, HNO_3, and SO_2, by wet-annular denuder air sampling with on-line chromatographic analysis. *Int. J. Env. Anal. Chem.* **1996**, *62*, 207–218.

(43) Febo, A.; Perrino, C.; Allegrini, I. Measurement of nitrous acid in Milan, Italy, by DOAS and diffusion denuders. *Atmos. Environ.* **1996**, *30*, 3599–3609.

(44) Genfa, Z.; Slanina, S.; Boring, B. C.; Jongejan, P. A. C.; Dasgupta, P. K. Continuous wet denuder measurements of atmospheric nitric and nitrous acids during the 1999 Atlanta Supersite. *Atmos. Environ.* **2003**, *37*, 1351–1364.

(45) Acker, K.; Moller, D.; Auel, R.; Wieprecht, W.; Kalass, D. Concentrations of nitrous acid, nitric acid, nitrite and nitrate in the gas and aerosol phase at a site in the emission zone during ESCOMPTE 2001 experiment. *Atmos. Res.* **2005**, *74*, 507–524.

(46) Bytnerowicz, A.; Sanz, M. J.; Arbaugh, M. J.; Padgett, P. E.; Jones, D. P.; Davila, A. Passive sampler for monitoring ambient nitric acid (HNO_3) and nitrous acid (HNO_2) concentrations. *Atmos. Environ.* **2005**, *39*, 2655–2660.

(47) Kleffmann, J.; Heland, J.; Kurtenbach, R.; Lörzer, J. C.; Wiesen, P. A new instrument (LOPAP) for the detection of nitrous acid (HONO). *Environ. Sci. Poll. Res.* **2002**, *9*, 48–54.

(48) Kanda, Y.; Taira, M. Chemiluminescent method for continuous monitoring of nitrous acid in ambient air. *Anal. Chem.* **1990**, *62*, 2084–2087.

(49) Takenaka, N.; Terada, H.; Oro, Y.; Hiroi, M.; Yoshikawa, H.; Okitsu, K.; Bandow, H. A new method for the measurement of trace amounts of HONO in the atmosphere using an air-dragged aqua-membrane-type denuder and fluorescence detection. *Analyst* **2004**, *129*, 1130–1136.

(50) Liao, W.; Hecobian, A. Mastromarino, J.; Tan, D. Development of a photo-fragmentation/laser-induced fluorescence measurement of atmospheric nitrous acid. *Atmos. Environ.* **2006**, *40*, 17–26.

(51) Pérez, I. M.; Wooldridge, P. J.; Cohen, R. C. Laboratory evaluation of a novel thermal dissociation chemiluminescence method for in situ detection of nitrous acid. *Atmos. Environ.* **2007**, *41*, 3993–4001.

(52) Dunlea, E. J.; Herndon, S. C.; Nelson, D. D.; Volkamer, R. M.; San Martini, F.; Sheehy, P. M.; Zahniser, M. S.; Shorter, J. H.; Wormhoudt, J. C.; Lamb, B. K.; Allwine, E. J.; Gaffney, J. S.; Marley, N. A.; Grutter, M.; Marquez, C.; Blanco, S.; Cardenas, B.; Retama, A.; Ramos Villegas, C. R.; Kolb, C. E.; Molina, L. T.; Molina, M. J. Evaluation of nitrogen dioxide chemiluminescence monitors in a polluted urban environment. *Atmos. Chem. Phys. Discuss.* **2007**, *7*, 569–604.

(53) Kebabian, P. L.; Herndon S. C.; Freedman, A. Detection of nitrogen dioxide by cavity attenuated phase shift spectroscopy. *Anal. Chem.* **2005**, *77*, 724–728.

(54) Triki, M.; Cermak, P., Mejean, G.; Romanini, D. Cavity Enhanced Absorption Spectroscopy with a LED source for NO_2 and NO_3 detection. *Appl. Phys. B* **2007**, submitted.

(55) Ball, S. M.; Langridge, J. M.; Jones R. L. Broadband cavity enhanced absorption spectroscopy using light emitting diodes. *Chem. Phys. Lett.* **2004**, *398*, 68–74.

(56) Kern, C.; Trick, S.; Rippel, B.; Platt, U. Applicability of light-emitting diodes as light sources for active differential optical absorption spectroscopy measurements. *Appl.Opt.* **2006**, *45*, 2077–2088.

(57) Sneep, M.; Ubachs, W. Direct measurement of the Rayleigh scattering cross section in various gases. *J. Quant. Spectrosc. Rad. Transfer* **2005**, *92*, 293–310.

(58) Baynard, T.; Lovejoy, E. R.; Pettersson, A.; Brown, S. S.; Lack, D.; Osthoff, H.; Massoli, P.; Ciciora, S.; Dube, W. P.; Ravishankara, A. R. Design and application of a pulsed cavity ring-down aerosol extinction spectrometer for field measurements. *Aerosol. Sci. Technol.* **2007**, *41*, 447–462.

Table 1. Parameters n_{HONO}, n_{NO2}, a, and b, and their associated fit uncertainties for different spectral fit windows (cf. eq 2) applied to measurements with chamber A. The values in bold correspond to the fit shown in Figure 3.

Range [nm]	$\boldsymbol{n_{HONO}}$ [10^{11} molecule cm^{-3}]	$\boldsymbol{n_{NO_2}}$ [10^{11} molecule cm^{-3}]	$\boldsymbol{a}$ [10^{-9} cm^{-1} nm^{-1}]	$\boldsymbol{b}$ [10^{-6} cm^{-1}]
366 – 371	9.7 ± 0.1	13.4 ± 1.0	18.8 ± 1.0	−6.9 ± 0.4
366 – 375	9.7 ± 0.2	10.6 ± 0.7	9.2 ± 1.2	−3.2 ± 0.4
366 – 378	**9.1 ± 0.2**	**10.6 ± 0.6**	**5.6 ± 1.1**	**−1.9 ± 0.4**
371 – 380	10.0 ± 1.0	11.1 ± 0.4	3.0 ± 0.6	−0.9 ± 0.2

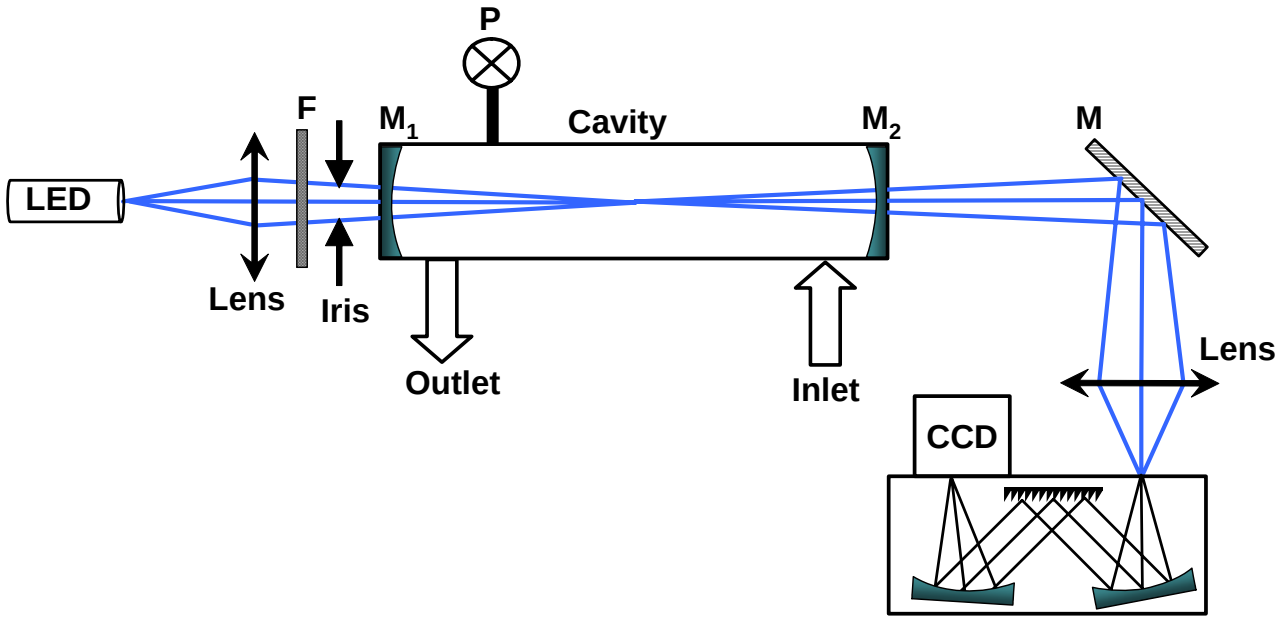


Figure 1. Schematic diagram of the experimental setup where LED is the light emitting diode, CCD is the charged coupled device, M is a metallic mirror, M_1 and M_2 are the high reflectivity dielectric mirrors centered at *ca.* 365 nm, F is a bandwidth filter, and P (chamber A) is a pressure gauge. The cavity length was 1.15 and 4.5 m for the two different gas chamber used in this study.

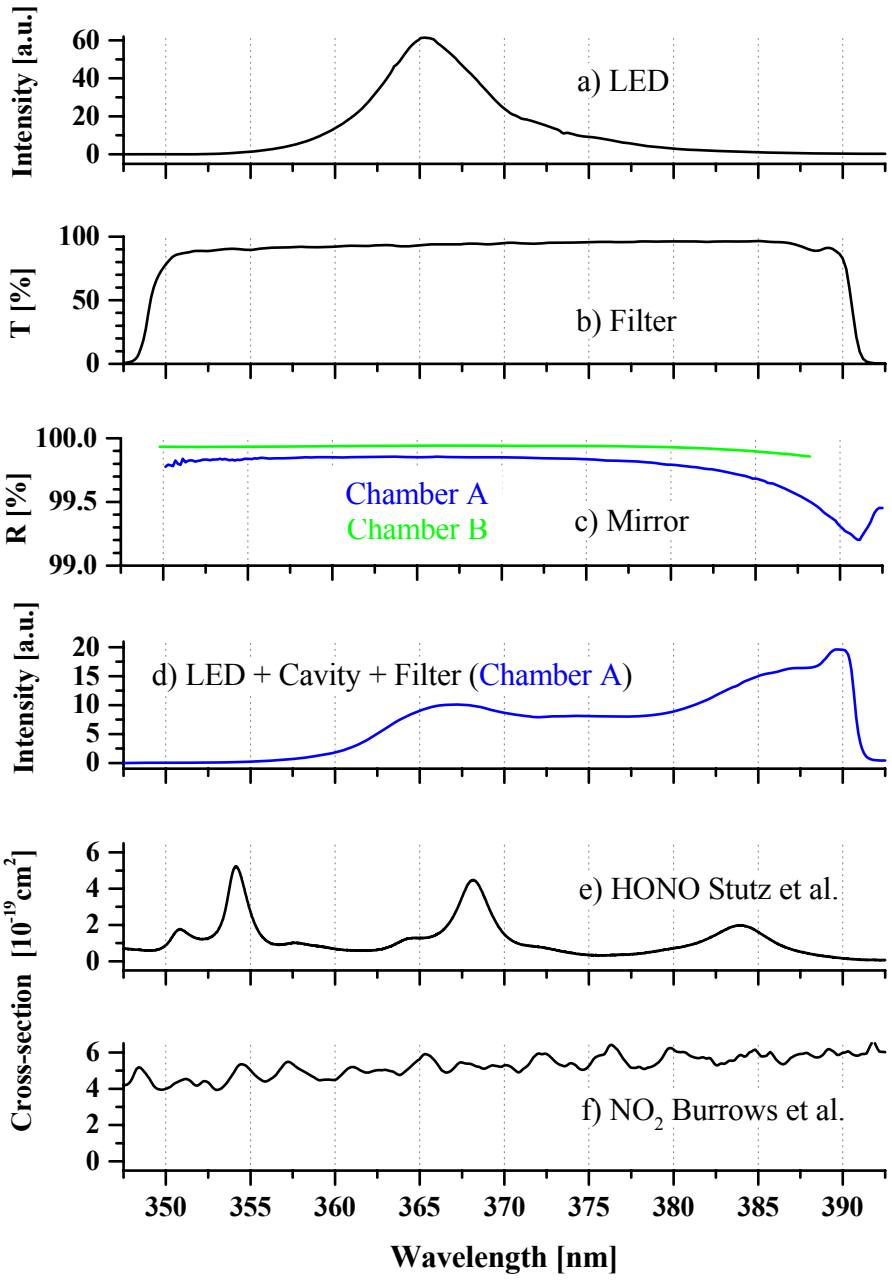


Figure 2. a) LED emission spectrum; b) filter transmission; c) Effective mirror reflectivity (smoothed) determined in chamber A and B experiments; d) empty cavity transmission spectrum (chamber A); e) HONO cross-sections by Stutz *et al.* (24); f) NO_2 cross-sections by Burrows *et al.* (25). Panels c) and d) refer to measurements with chamber A only.

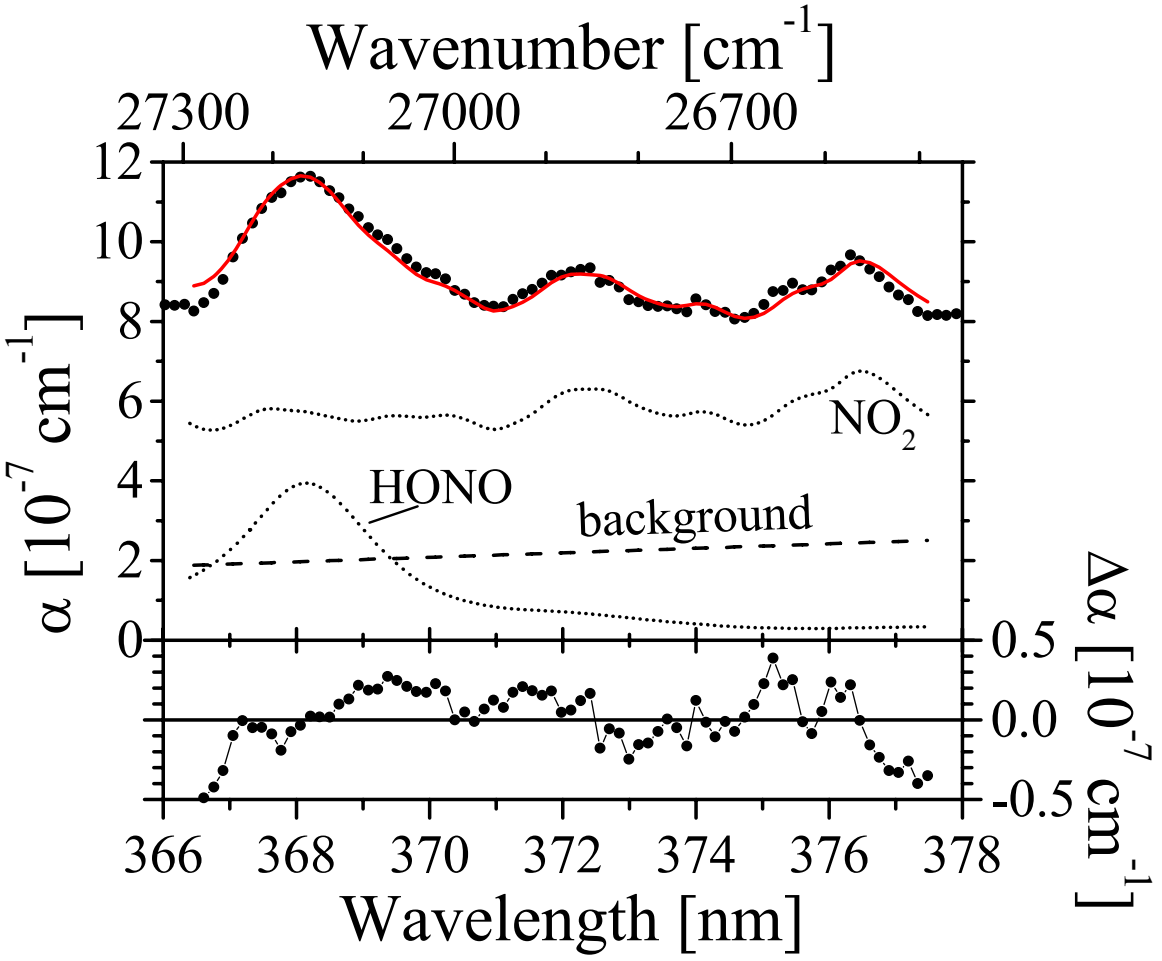


Figure 3. Upper panel: Absorption coefficient of a mixture of HONO and NO_2 (solid circles) from 364 nm to 378 nm measured with chamber A at *ca.* 25 mbar pressure using an acquisition time of 20 s (for details see experimental section). The red line was determined by a non-linear least square fit of eq 2 to the measured data. The number densities for HONO and NO_2 found in the fit were $(9.1 \pm 0.3)\times10^{11}$ cm^{-3} and $(10.6 \pm 0.7)\times10^{11}$ cm^{-3}, respectively. The linear background found in the fit is indicated by a straight dashed line (a = 5.67×10^{-9} cm^{-1} nm^{-1}, b = -1.89×10^{-6} cm^{-1}). The dotted spectra represent the absorption coefficients of HONO and NO_2 according to their contributions to the overall fit. Lower panel: Absolute residuals of the fit, $\Delta\alpha$.

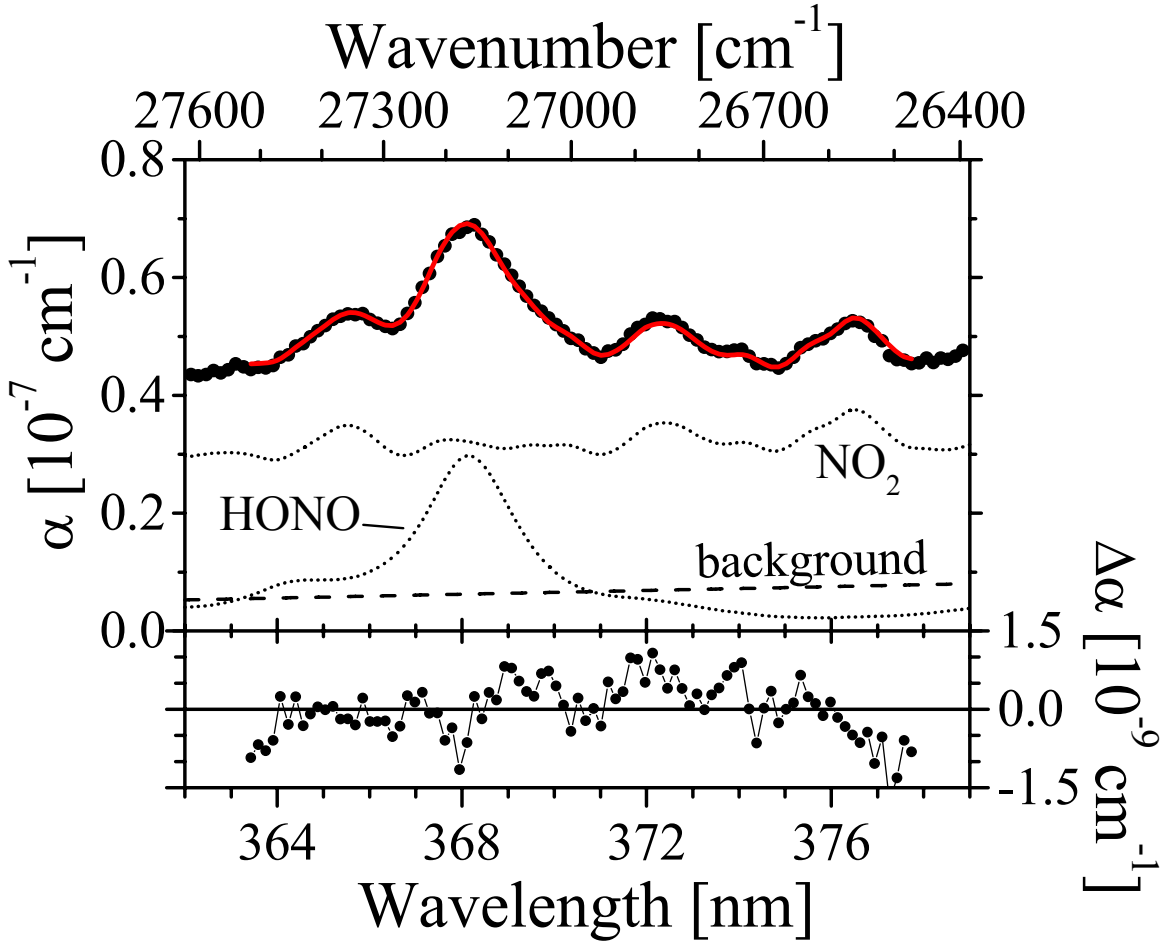


Figure 4. Upper panel: Absorption coefficient of a mixture of HONO and NO_2 (solid circles) from 362 nm to 379 nm measured with chamber B at *ca.* 1010 mbar using an acquisition time of 10 min. The red line was determined by a non-linear least square fit of eq 2 to the measured data. The number densities for HONO and NO_2 found in the fit were $(67.4 \pm 1.2)\times10^{9}$ molecule cm^{-3} and $(58.2 \pm 0.4)\times10^{11}$ molecule cm^{-3}, respectively. The linear background found in the fit is indicated by a straight dashed line ($a = 1.61\times10^{-10}$ cm^{-1} nm^{-1}, $b = -53.3\times10^{-9}$ cm^{-1}). The dotted spectra represent the absorption coefficients of HONO and NO_2 according to their contributions to the overall fit. Lower panel: Absolute residuals of the fit, $\Delta\alpha$.